# Wirelessly Powered 3-D Printed Headstage Based Neural Stimulation System for Optogenetic Neuromodulation Application

Dipon K. Biswas, *Student Member, IEEE*, Nabanita Saha, and Ifana Mahbub, *Senior Member, IEEE*

***Abstract*—This work presents a miniaturized wireless power transfer (WPT) system integrated with a neuromodulation headstage for duty-cycled optical stimulation of freely moving rodents. The proposed WPT system is built using the commercially available off-the-shelf components (COTS) for the optogenetic neuromodulation system consisting of a bridge rectifier, a DC-DC converter, an oscillator circuit, an LED driver, and a $\mu$LED. The total power consumption of the stimulation system is 14 mW which is provided using the WPT method. The WPT system includes a novel transmitter (TX) coil implemented on a printed circuit board (PCB), and a solenoid receiver (RX) coil wrapped around a customized 3-D printed headstage. The proposed TX coil is designed in such a way that the magnetic field all across the TX coil is sufficient to provide the required power to the optical stimulation system that is worn as a headstage by the freely moving rat. The headstage device's dimension is 18.75 mm $\times$ 21.95 mm, weighing 4.75 g. The ratio of the weight of the headstage and rat is 4.75:300. The proposed system is able to achieve a maximum overall efficiency of $\sim$63% at 5 cm separation between the TX and RX coils, where the maximum power transfer efficiency (PTE) of the WPT system is $\sim$88% and the power conversion efficiency (PCE) of the rectifier is 71.6%. The proposed system with reconfigurable stimulation frequency is suitable for exciting different brain areas for long-term health monitoring.**

***Index Terms*—Efficiency, inductive link, optogenetic neuromodulation, wireless power transfer.**

## I. Introduction

WIRELESS power transfer (WPT) system introduces a new pathway for transferring continuous power to the low-power circuits such as implantable medical devices, where replacement of batteries is difficult, and the space is limited. The treatment of these neurological disorders exploits brain stimulation techniques such as magnetic seizure therapy (MST), deep brain stimulation (DBS), etc [1]. The proposed wireless power transfer (WPT) technique eliminates the bulky wires and batteries attached to the animals for optogenetic neuromodulation application and thus enables long-term behavioral studies. In this work, a reconfigurable pulse stimulation system is employed which makes the system suitable for the stimulation in different deep brain regions such as the subthalamic nucleus, thalamus, etc. [2]. The optogenetic device is powered up wirelessly using a TX coil which is connected to a signal generator and placed under the floor of the behavioral cage. In our prior works, a headstage-based WPT system is developed to provide continuous power to the stimulation circuit all across the behavioral cage [3], [4]. However, the proposed TX coil architecture had some blind spots where the system was not able to provide enough power for the stimulation.

In this work, a novel TX coil architecture is proposed that improves the magnetic field distribution and eliminates the blind spots. Prior research works also present the use of headstage-based neural stimulation system for freely moving rats [5], [6], [7]. In [5], magnetic resonance techniques were proposed to power the stimulation system where the maximum distance between the TX and RX coils was 2 cm only. In [8], a transmitter-receiver (TX-RX) flexible printed coil (FPC) array has been proposed for the WPT system which features dual resonance responses. However, it is not suitable to be implemented for freely moving animal experiments because of the large size of the receiver coil.

In this work, we have demonstrated a novel WPT system with a novel TX coil architecture and a reconfigurable optogenetic stimulation capability integrated inside a headstage. The contribution of this work is the unique configuration of the turn in the spiral antenna to design an optimized WPT system. This system have achieved a maximum PTE of 88% with a smaller receiver size and this PTE is comparatively higher than the previous works. The proposed system eliminates the use of the battery while being able to achieve a 5 cm distance for powering up the neuromodulation system. The novelties of this work are: i) the consideration of the various brain tissue layers in the optimization process of the TX and RX coils' sizing, which improved the accuracy of the optimization process compared to the prior works, ii) the configuration of the turn in the spiral antenna, which resulted in the overall enhancement of the total generated flux, PTE, and PCE compared to the other works, iii) optimizing the transmission distance, and iv) smaller receiver

Manuscript received 6 July 2022; revised 6 September 2022 and 26 October 2022; accepted 24 November 2022. This work was supported by the National Science Foundation (NSF) under Grant ECCS 1943990. *(Corresponding author: Ifana Mahbub.)*

Dipon K. Biswas is with the Department of Electrical Engineering, University of North Texas, Denton, TX 76203 USA (e-mail: diponkumarbiswas@my.unt.edu).

Nabanita Saha and Ifana Mahbub are with the Department of Electrical and Computer Engineering, University of Texas at Dallas (UTD), Richardson, TX 75080 USA (e-mail: nabanitasaha@my.unt.edu; ifana.mahbub@utdallas.edu).

Digital Object Identifier 10.1109/JERM.2022.3225972

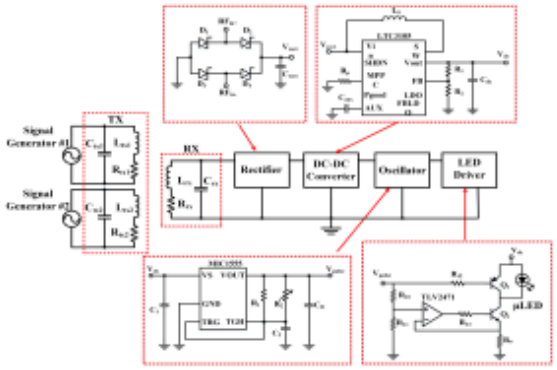


Fig. 1. Overview of the proposed wirelessly powered neural stimulation system.

size (167.41x smaller than the transmitter) and the elimination of the need for using multiple resonators. The diameter of the proposed receiver coil is 18.75 mm only, which is much smaller than the receivers of previous works. The paper is organized as follows: Section II discusses the detailed design architecture of the WPT system, followed by Section III which presents the optimization technique of the WPT system. Section IV presents the simulated and experimental results, followed by a concluding remark in Section V.

## II. System Overview

The complete optogenetic neuromodulation system is powered using a WPT method which includes a transmitter (TX) coil and a receiver (RX) coil as shown in Fig. 1. The TX coil is modeled as two parallel RLC circuits. One coil is denoted as $L_{TX1}$, $R_{TX1}$, and $C_{TX1}$, and the other coil is denoted as $L_{TX2}$, $R_{TX2}$, and $C_{TX2}$, where $L$, $R$, and $C$ indicate inductor, resistance, and resonating capacitor, respectively [9]. Similarly, the RX coil is also modeled as an RLC circuit represented as $L_{RX}$, $R_{RX}$, and $C_{RX}$. An $L$-shape matching network is added to each of the TX coil to match the impedance of the TX coil (133 Ω) with 50 Ω signal generator. A $Pi$-shape matching network is used after the RX coil to match the impedance of the coil (78 Ω) to the impedance of the rectification circuitry (116 Ω).

### A. Transmitter Coil

The proposed transmitter (TX) coil is a cascaded two-layer planar spiral coil fabricated using a copper conductor on an FR4 substrate (dielectric constant, $\epsilon_r$ of 4.3 and loss tangent, tan$\delta$ of 0.02). The total dimension of the TX coil is 215 mm × 215 mm with a 1.6 mm substrate thickness, which matches the dimension of the behavioral cage of the rodent. The complete TX board consists of two identical TX coils which are fed separately using two external RF sources. Two RF power amplifiers (PA) (SMAKN 2MHz-700MHz, 3 W amplifier) with a 15 dB gain are used to drive the TX coils. The PA has a maximum bias voltage of 8.5 V which provides a 22 dBm output power when the input power is 7 dBm. As the PAs are terminated with a 50 Ω matched

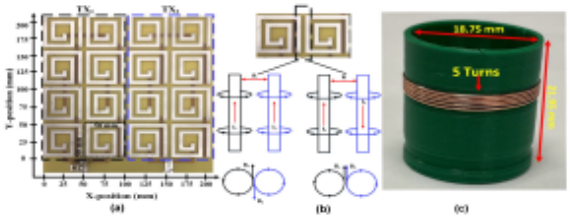


Fig. 2. (a) Fabricated transmitter (TX) coil, (b) Magnetic field concept for two parallel wires when current is flowing in the same and opposite direction. (c) Fabricated receiver (RX) coil architecture.

port, a matching network is required in between each PA and the TX coil. An $L$-shape matching network consisting of 42 nH inductor and 3300 pF capacitor is designed to match the input impedance of the TX with a 50 Ω port. A resonating capacitor of 82 pF is used to resonate each TX coil to 13.56 MHz. Both of the TX coils are designed to have a series of eight-unit spiral coils. The unit spiral coil is a 2-turn square spiral with a total dimension of 50 mm × 50 mm, and a trace width/spacing of 5 mm as shown in Fig. 2(a). The dimension of the unit cell is determined through an optimization algorithm implemented using Python language, which is detailed in Section III [10]. The unit cells are connected according to the Curl right-hand rule so that the current flowing through the unit cell is in the opposite direction for the adjacent unit cells which enhances the magnetic field [11]. As shown in Fig. 2(b), the current is flowing in the same direction which results in two magnetic fields $\vec{B}_1$ and $\vec{B}_2$ in the opposite direction. The values of the magnetic fields $\vec{B}_1$ and $\vec{B}_2$ can be defined as (1) and (2) [12].

$$\vec{B}_1 = \frac{\mu_0 \vec{I}_1}{2\pi\frac{R}{2}} = \frac{\mu_0 \vec{I}_1}{\pi R} \tag{1}$$

$$\vec{B}_2 = \frac{\mu_0 \vec{I}_2}{\pi R} \tag{2}$$

Here, $\vec{I}_1$, and $\vec{I}_2$ are the current flowing through the conductors, $R$ is the distance between the two parallel conductors, and $\mu_0$ is the relative permeability of free space ($4\pi \times 10^{-7}$ H/m.) The total magnetic field is a vector summation of the two magnetic fields, $\vec{B}_1$and $\vec{B}_2$ as shown in (3).

$$\vec{B} = \vec{B}_1 + \vec{B}_2 \tag{3}$$

With the same current flowing through the parallel conductors in the same direction, the two magnetic fields cancel each other, thus weakening the total magnetic field in the center of the two conductors. On the other hand, when the currents flow in the opposite direction, the overall magnetic field in between the conductors is enhanced as shown in Fig. 2(b).

### B. Fabrication of Receiver Coil and Headstage

The proposed RX coil is a 5-turn coil designed using 38 AWG Remington wire. It is wrapped around a 3D printed headstage which is fabricated using the Creality Ender 3. The headstage is cylindrical in shape with 18.75 mm outer diameter

and 21.95 mm height, and with a wall thickness of 1 mm. The proposed RX is also designed and simulated using the Ansys HFSS (version 2021.1.0 R1) with the PLA (Polylactic acid) substrate with a dielectric constant of ∼2.8 and a dielectric loss of $\sim 10^{-1}$ at room temperature [13]. The fabricated headstage with the RX coil is shown in Fig. 2(c).

### C. Bridge Rectifier

The proposed rectifier circuit is a bridge rectifier architecture that uses a PMEG2020AEA Schottky diode (Nexperia USA Inc.). The proposed Schottky diode has a minimum forward voltage requirement of 450 mV and a maximum forward current of 2A [14]. During the negative half-cycle, the capacitor, $C_R$ discharges through a 3 kΩ load resistor which is the equivalent resistance of the DC-DC converter, oscillator, and $\mu$LED. The value of the capacitor, $C_{rect}$ is set to 220 $\mu$F to remove the output ripples.

### D. DC-DC Boost Converter

To provide the required constant 3.3 V supply voltage to the $\mu$LED, a commercial DC-DC converter is used after the bridge rectifier. The proposed DC-DC converter is a highefficiency step-up DC-DC converter (LTC3105) by Linear Technology which has a start-up voltage of 250 mV. The input voltage range of the proposed DC-DC converter can vary from 225 mV to 5 V. The DC-DC converter is a 10-lead 3 mm × 3 mm DFN packaged chip. To set the lowest input value of 250 mV, the value of $R_p$ is chosen to be 25 kΩ. A feedback resistive divider consisting of $R_1$ and $R_2$ is used at the output node that helps to adjust the output voltage between 1.6 to 5.25 V. To get a 3.3 V at the output node, the calculated values for $R_1$ and $R_2$ are chosen as 1.02 MΩ and 200 kΩ, respectively. A load capacitor, $C_{dc}$ of 10 $\mu$F is chosen to get rid of the output ripples.

### E. Oscillator Design for the Duty-Cycled Stimulation

The oscillator circuit includes a commercially available MIC1555 CMOS RC oscillator by Microchip to provide pulses with a precise frequency to the $\mu$LED in this work. The MIC1555 has a SOT-23 package that can be powered from a 2.7 to 18 V supply voltage. An input capacitor, $C_1$ of 1 $\mu$F is used to decouple the input noise. The oscillator can act as a monostable or as an astable oscillator. To use the MIC1555 as an astable oscillator, the trigger (TRG) and the threshold (THG) pin need to be connected. To set the output frequency in the astable mode, the output RC components need to be adjusted according to (4).

$$f = \frac{1}{K_1 RC} \tag{4}$$

where $R$ is the equivalent resistance of the output parallel resistance $R_1$ and $R_2$, and $C$ is the threshold capacitance, $C_2$, as shown in Fig. 1. $k_1$ is a constant which has a constant value of 1.42 for the $RC$ constant range of 0.01 s to 0.1 s. In this work, a fixed resistance of 220 kΩ is used as $R_1$ resistance and a 1 $\mu$F capacitor is used as the threshold capacitor. To make the oscillator reconfigurable, a variable resistor $R_2$ having a resistance range of 10–110 kΩ is used, and a load capacitor $C_o$ of 100 pF is used to make the output pulse smoother.

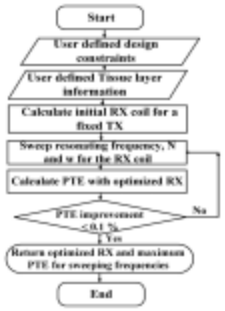


Fig. 3. Detailed flowchart of the optimization process.

### F. LED Driver Circuitry

An LED driver circuit is used after the oscillator. The LED driver circuit shown uses a current source that is based on a closed-loop op-amp, TLV2471 for ensuring the right amount of current is passed through the LED. To control the current through the LED, one NPN (BC817) transistor and one PNP (BC857) transistor are used which are denoted by $Q_1$ and $Q_2$, respectively, as shown in Fig. 1. Such an op-amp-based current source provides a fixed voltage on the emitter of $Q_1$, which guarantees a fixed current through a precision resistor, $R_9$ with a value of 0.5 Ω. An LB-QH9G $\mu$LED by OSRAM Opto-semiconductors (minimum forward voltage of 2.7 V and a minimum forward current of 5 mA) is connected in parallel to the transistor, $Q_1$.

## III. Optimization Method of the WPT System

The steps of the proposed optimization method are shown in a flowchart in Fig. 3. For the optimization of the coil design to achieve the maximum efficiency taking into account all the design constraints (e.g., maximum allowable size, trace width, spacing, tissue losses), an optimization algorithm and tool is developed using the Python language. Unlike the conventional optimization approach, where the frequency is usually a user-defined input, the proposed optimization tool inputs the frequency as a variable and the efficiency is maximized by computing the optimum frequency. [10]. At first, the design constraints such as coil dimensions, frequency range, fabrication constraints, the distance of operation are provided by the user followed by brain tissue layer information. The tissue layer information includes the relative permittivity, $\epsilon_r$, and conductivity, $\sigma$ of each brain tissue layer. The TX size is kept constant as a design constraint.

In the next step, the frequency is swept over the user-defined frequency range to find the maximum PTE for the optimized RX coil. For each of the frequency points, the number of turns $N$ and width $w$ of the RX coil is calculated to find the maximum PTE. After these iterative steps, if the efficiency of the system improves by more than 0.1%, then the process goes back to

TABLE I
TISSUE LAYER PROPERTIES

| Tissue layer | Relative permittivity, $\epsilon_r$ | Conductivity, $\sigma$ (S/m) | Thickness, (mm) |
|---|---|---|---|
| Skin | 36 | 0.69 | 1 |
| Skull | 12 | 0.16 | 2 |
| Greymatter | 48 | 0.83 | 57 |

step 5 to continue the iteration until the efficiency improvement is less than 0.1%. Similar iterations take place for each frequency point in the frequency range provided by the user and then the frequency point that results in the maximum PTE is returned along with the TX and RX coil dimensions. The proposed optimization method is an iterative process based on the mutual coupling between the TX and RX coils. The script is written in Python language based on the coupling equation presented in [15]. With the current conditions, the optimization process requires 1083 passes to converge. Here, the convergence time is 169 seconds, and the number of iterations is 512. The number of passes to converge can vary depending on the frequency range and step size. The variation in the modeled and simulation results is due to the limited information regarding the copper plated through-hole vias of the FR-4 based TX coil which has not been incorporated with much precision.The through-hole connection is required for the eight unit cells connected in series.

As the RX coil needs to be wrapped around the headstage module, the diameter of the solenoid-based coil is kept constant to 18.75 mm. The optimization process is designed keeping in mind that the TX coil will be an array-based design. The outer dimension of TX coil is kept fixed due to the size constraint. The TX coil is designed in such a way that its dimension matches the dimension of the behavioral cage. As a result, the unit cell dimension of the array-based TX coil is kept to a constant value which is in this case 50 mm $\times$ 50 mm. This dimension is determined from the total dimension of the behavioral cage of the rat for the in-vivo experiment. The distance is also set to be 5 cm as the height of the rat's head from the ground can be as high as 5-6 cm. The optimization is performed to optimize the trace-width and number of turns without changing the outer diameter of the TX unit cell. The tissue layers of the rat's head are realized as skin (1 mm)-skull (2 mm)-greymatter (44 mm)-skull (2 mm)-skin (1mm) layers [16]. The detailed information of the tissue layers is presented in Table I. The optimization process uses a frequency range of 1–20 MHz to find out the maximum PTE.

The optimization method is run four times for four different TX coils and the acquired PTE results are shown in Fig. 4. The number of turns of the unit cell of the TX coil is varied from 2 to 5-turns with a step of 1 turn while the diameter of the TX is kept constant to 50 mm $\times$ 50 mm. For each TX coil combination, the number of turns of the RX coil is swept from 2 to 7-turns. Fig. 4 shows the optimized PTE results for the TX coil with 2, 3, 4, and 5 turns, respectively. According to these results, the RX coil with 5 turns shows the maximum PTE for each combination compared to the other combinations, the maximum PTE is found to be 96.8% at

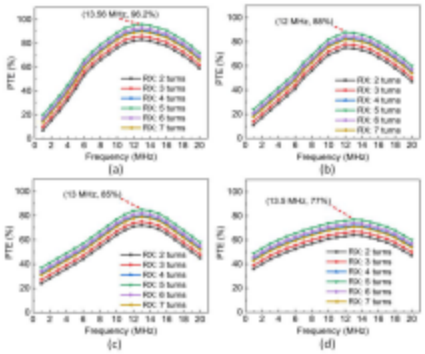


Fig. 4. Optimized PTE for several RX coils, when (a) the TX coil unit cell is 50 mm $\times$ 50 mm with 2 turns, (b) the TX coil unit cell is 50 mm $\times$ 50 mm with 3 turns, (c) the TX coil unit cell is 50 mm $\times$ 50 mm with 4 turns, and (d) the TX coil unit cell is 50 mm $\times$ 50 mm with 5 turns.

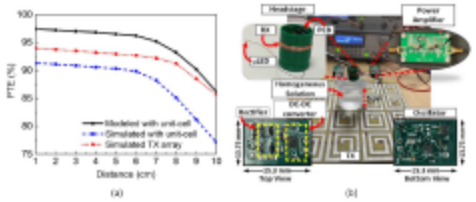


Fig. 5. (a) Comparison of the modeled and simulated PTE for the combination of a unit cell of the TX coil and proposed RX coil to the combination of arraybased TX coil and the proposed RX coil (b) Complete test-bench setup with a detailed figure of the PCB boards.

13.5 MHz when the TX coil has 2-turns and the RX coil has 5-turns as shown in Fig. 4(a). Thus, the proposed RX coil is chosen to have 5 turns and the unit cell of the TX coil is chosen to be 50 mm $\times$ 50 mm with 2 turns. A performance comparison is analyzed between the theoretically modeled and the simulated TX and RX coil combinations. The unit cell of the TX coil and the proposed RX coil are designed and the tissue medium between the TX and RX coils are also modeled in HFSS. As shown in Fig. 5(a), the theoretically modeled PTE varies from 87% to 96% over the distance of 1–10 cm at 13.56 MHz. The simulated results show a PTE variation of 77% to 92% for the same distance range. However, to cover the whole area of a behavioral cage for invivo experiments, the total dimension of the TX coil is chosen to be 215 mm $\times$ 215 mm, which includes a series combination of the optimized unit cells. Thus, a simulation is performed with the TX coil and the proposed RX coil to validate the performance of the TX coil array. The result in Fig. 5(a) shows that the PTE varies from 86% to 94.2% over the varying distance of 1–10 cm.

## IV. IMPLEMENTATION AND MEASUREMENT RESULTS

The total neuromodulation system is divided into two sections: i) WPT system, and ii) the optical stimulation system. The complete test-bench setup is shown in Fig. 5(b). To measure the

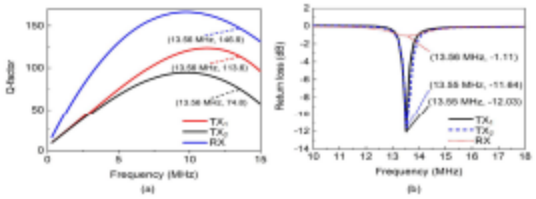


Fig. 6. (a) Measured Q-factor of the fabricated TX and RX coil, (b) Return losses of the proposed TX and RX coils.

PTE, the headstage is placed at the center of the sixteen unit cell and 5 cm apart from the TX coil.

### A. *Wireless Power Transfer System*

The WPT system includes two identical TX coils and a solenoid-based RX coil. All the coils are designed to resonate at 13.56 MHz which is in the ISM band (industrial, scientific, and medical) that is dedicated for animal-related experiments by Federal Communications Commission (FCC). The $Q$- factor can be calculated as:

$$Q = \sqrt{\frac{X_L}{X_C}}\,\frac{1}{R} \tag{5}$$

where $R$ represents an internal resistance of each inductor, $X_L$ *represents the inductance, and* $X_C$ represents the capacitance. Fig. 6(a) shows the $Q$-factor of the proposed TX coils and the RX coil. Though the two TX coils are designed to be identical, the $Q$-factors at 13.56 MHz are 113.6 and 74.8 for the $TX_1$ and $TX_2$, respectively. The precision of the fabrication and the amount of soldering used for integrating the SMA connector might be the reason behind this discrepancy. The $Q$-factor of the complete system with a single feeding network is found to be 76.3 at 13.56 MHz, which is comparable to the TX coils with parallel feeding networks. The $Q$-factor of the RX coil is measured to be 146.9 at 13.56 MHz. The PAs are connected to Keysight 33210A function generators to drive the TX coils.

The return losses of the TX coils are shown in Fig. 6(b) where results below $-10$ dB at 13.56 MHz indicate that the TX coils are well-matched with the impedance of the PA output. The RX coil is also resonated at 13.56 MHz with a resonating capacitor of 181 pF when the load resistance of the RX coil is 600 Ω which emulates the impedance of the LED. The return loss of the RX coil is $-1.11$ dB at 13.56 MHz as shown in Fig. 6(b). The poor return loss value is due to the fact that the load resistance value is not the optimum value. PTE of a WPT system is the ratio of the RF output power to the RF input power for the WPT link [17].

$$PTE = \frac{P_{RFout}}{P_{RFin}} \times 100\% \tag{6}$$

The PTE of the proposed WPT system is given by,

$$\frac{P_{RFout}}{P_{RFin}} = 10^{\frac{|S_{21}|}{10}} \tag{7}$$

where $S_{21}$ is the transmission coefficient from port 1(TX coil) to port 2 (RX coil). To find out the optimum load resistance value

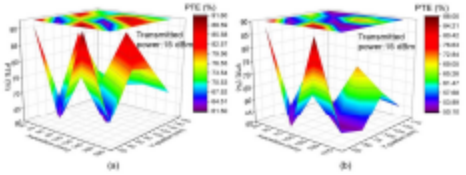


Fig. 7. (a) Simulated PTE over the proposed TX coil at a 5 cm distance (b) Measured PTE over the proposed TX coil at 5 cm distance.

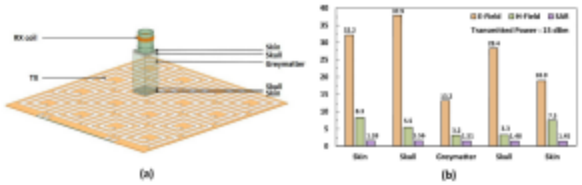


Fig. 8. (a) Modeled tissue layer in HFSS, (b) Simulated E-field, H-field, and SAR values.

for the maximum PTE for the proposed WPT system, the load resistances are varied from 1 to 10 kΩ in the simulation using Keysight Advanced Design System (ADS) (version 2021.02). For the ADS simulation, the measured S2P file of the TX and RX system is imported to ADS. The maximum PTE is achieved to be 62.89% at a 5 cm distance between the TX and RX coils when the load resistance is 3 kΩ. Hence, a matching network is designed to match the impedance of the LED to 3 kΩ.

A Pi-shape CLC (Capacitor-Inductor-Capacitor) matching network is designed on the RX coil end having the values of 3 pF capacitance and 1 nH inductance to match with the 3 kΩ resistance. With the matching network, at 13.56 MHz, the RX coil achieves -12.07 dB return loss which is measured using the Keysight E5061B Vector Network Analyzer (VNA). To further characterize the WPT system, the PTE of the proposed TX and RX coils is simulated using the Ansys HFSS. For measurement purposes, a homogeneous solution is prepared to mimic the five tissue layers. A sucrose-based solution consisting of NaCl, sugar, agar, benzoic acid, ($C_6H_5COOH$), and water is used to prepare the homogeneous tissue-mimicking solution according to the dielectric phantom recipe provided by the National Institute of Health (NIH) website [18]. The solution was prepared in a cup to mimic the 5 cm tissue layer for the measurement set-up. We already experimentally verified the dielectric constant of the tissue-mimicking solution in [16]. To perform the simulation on various positions of the TX coils, the TX board is segmented along with its width, and length, and the RX coil is placed 5 cm apart from the TX coil. As shown in Fig. 7(a), the contour plot indicates the PTE of the WPT system where the X-position indicates the width of the TX coil, and the Y-position indicates the length of the TX coil in mm. To emulate the rat's head, the modeled tissue layer which consists of skin, skull, greymatter, skull, skin as shown in Fig 8(a) is used in the simulation. The RX coil is placed 5 cm apart from the TX coil on sixteen selected positions which are centered on each of the unit cells of the TX coil. The maximum PTE achieved in the simulation is 93.50% and the minimum PTE is simulated to be 64% which are shown

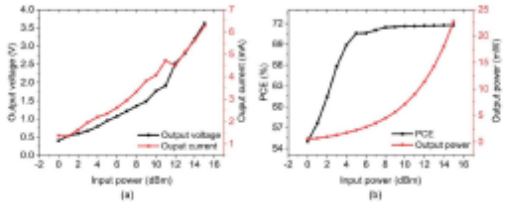


Fig. 9. (a) Measured output voltage and current of the proposed rectifier for various input power, (b) Measured power conversion efficiency (PCE) and the output power of the proposed architecture.

in Fig. 7(a). The measurement results in Fig. 7(b) show that the PTE varies from 50.4% to 87.9% all across the TX coils.

With the minimum PTE of 50.4% at (125 mm, 75 mm) position, the RX coil receives 12.5 dBm (17.7 mW) when the transmitted power is 15 dBm (38.56 mW). While transmitting power wirelessly to the RX coil, the analysis of the maximum E-field, H-field, and Specific Absorption Rate (SAR) for the safety of the surrounding tissue is also analyzed using Ansys HFSS. The simulated model is designed to emulate the measurement setup where the headstage is mounted on top of the mouse's head and the TX coil is placed on the floor of the behavioral cage. The distribution of E-field, H-field, and SAR through the brain tissue layers is shown in Fig. 8(b). The maximum E-field through the skin layer is 32.2 V/m, and it is 37.9 V/m and 13.2 V/m through the skull and Greymatter layers, respectively, when the transmitted power is set as 15 dBm. A maximum H-field of 8.3 A/m is found through the skin layer. With the increase in the tissue layer thickness, the H-field decreases as the coupling between the TX and RX coils decreases over the distance. The values don't exist the radiation dosimeter for the rats [19]. The SAR is a function of the electric field generated by the TX coil which follows (8).

$$SAR = \frac{\sigma |E|^2}{\rho} W/kg \tag{8}$$

Here, $\sigma$ is the conductivity of the tissue layer, $\rho$ is the density of the tissue layer, and $E$ is the electric field induced in the tissue layer. The maximum simulated SAR achieved in this experiment is 1.57 W/kg through the skin layer for 15 dBm transmitted power which is within the Federal Communication Commission (FCC) regulations. The maximum allowable SAR value through the tissue layer is 1.6 W/Kg [20].

### B. Optical Stimulation

The optical stimulation system consists of the bridge rectifier circuit that converts the received AC power to DC power. Measurement results show that for an input power of 0 dBm to 15 dBm, the output voltage at the output of the rectifier is in the range of 0.4–3.6 V, as shown in Fig. 9(a). The bridge rectifier is able to provide a maximum of 6.5 mA current for 15 dBm input power. Based on the input AC power and the output DC power, the total power conversion efficiency (PCE) is defined as

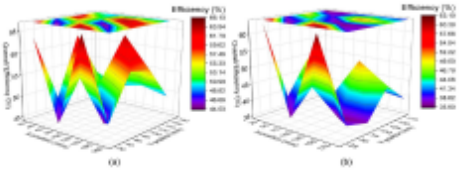


Fig. 10. (a) The simulated overall efficiency of the system over the proposed TX coil at a 5 cm distance (b) Measured Simulated overall efficiency of the system over the proposed TX coil at a 5 cm distance.

(9).

$$PCE\,(\%) = \frac{P_{outDC}}{P_{inAC}} \times 100\% \tag{9}$$

The overall efficiency, $\eta$ of the neuromodulation system is calculated from the PTE of the WPT system and multiplying with the PCE of the rectifier circuitry, as shown in (10).

$$\eta\,(\%) = \frac{(PTE \times PCE)}{100} \tag{10}$$

A PCE of 55% is achieved at 0 dBm input power which delivers 0.5 mW of power to the load as shown in Fig. 9(b). As the minimum required power for $\mu$LED is 14 mW, obviously, a higher input power is needed at the input of the rectifier. For the input power of 13 dBm, the rectifier achieves 71.6% PCE, which results in an output power of 14.3 mW with a 3 k$\Omega$ load resistance, which is enough for the LED to provide at least 5 mW/$mm^2$ luminosity [21]. The output voltage of the rectifier is regulated to 3.3 V using the commercial DC-DC voltage converter. The output voltage of the DC-DC converter is also used as the input supply voltage for the MIC1555 oscillator which has the capability to achieve a reconfigurable pulse signal for stimulation.

In this work, a 20 Hz oscillation frequency with a voltage amplitude of 3.3 V is used to drive the $\mu$LED. The overall efficiency, $\eta$, of the neuromodulation system is calculated from Fig. 10(a) and (b), which show the simulated and measured overall efficiencies of the complete system, respectively. The efficiency is calculated for a fixed PCE value of 71.6% which aais the maximum value achieved by the rectifier. Th stimulated overall efficiency shows a maximum efficiency value of 67% [Fig. 10(a)]. On the other hand, the maximum measured efficiency is 63% as shown in Fig. 10(b). In our prior work [26] the system with a multilayer planar TX coil array (where the current is flowing through the unit cell in the same direction) is able to achieve a maximum of 41.7% efficiency at a 5 cm distance. The proposed work can achieve a maximum overall efficiency of 63% at 5 cm separation between the TX and RX coils, where the maximum power transfer efficiency (PTE) of the WPT system is 88%.

Table II presents a comparison of the performance parameters of the other works with those of this work. In most of the prior works, a 4-5 coil system is used with resonator coils along with the RX coil to enhance the electromagnetic field. In [24], the author proposed a system that achieves 36.3% PTE at 7 cm distance. Though the distance is higher compared to the

TABLE II
COMPARISON WITH THE STATE-OF-THE-ART

| Parameters | This work | [22] | [23] | [24] | [25] |
|---|---|---|---|---|---|
| Frequency (MHz) | 13.56 | 13.56 | 300 | 13.56 | N/A |
| RX size coil | 18.75 mm diameter | 29 mm diameter | 43 mm × 38 mm | 25 mm diameter | 60 mm × 80 mm |
| Coil coupling | 2-coil | 4-coil | Square-patch | 5-coil | 2-coil |
| TX size coil | 215 mm × 215 mm | 270 × 270 mm | 43 mm × 38 mm | 300 mm × 300 mm | 200 mm × 200 mm |
| Distance | 5 cm | 4 cm | 2.2 cm | 7 cm | N/A |
| Maximum PTE (%) | 88 | 69 | 70.1 | 36.3 | 88.4 |
| Maximum efficiency (%) | 63 | 48.3 | NA | 26.86 | 80.9 |

proposed system, the PTE is lower compared to the achieved 88% efficiency. Moreover, the prior work also used a 5-coil system, yet achieved lower overall efficiency compared to 63% efficiency. In [25], the author presented higher overall efficiency for the 2-coil system compared to the proposed work, which includes a single RX coil. However, the RX coil size is much larger compared to the proposed system. With a lower footprint of the RX coil, the proposed system is still able to achieve the highest PTE compared to the prior works.

## V. CONCLUSION

This paper presents the complete wirelessly powered, optogenetic neuromodulation system for neuromodulation application which can stimulate neurons with reconfigurable light pulses. The system uses a reconfigurable stimulation technique that allows the system to stimulate and record from different brain regions. The proposed WPT system uses parallel TX coils with parallel feeding networks which reduces the overall resistance and increases the $Q$-factor, thus enhancing the magnetic field. This proposed WPT system has a novel TX coil architecture with a reconfigurable frequency control capability which improves the magnetic field distribution and eliminates the blind spots of the previous works. The contributions of the proposed work are the optimization and modeling techniques which made the WPT system highly efficient with a PTE of 88% and the rectification circuitry achieves a maximum of 71.6% PCE. The current version indeed requires manual adjustment, but with a variable resistor on-chip where we can control the resistance digitally, we can wirelessly control the parameters with a bi-directional wireless communication system. The future work includes the design of a miniaturized and fully implantable WPT system for non-invasive or subinvasive optogenetic neuromodulation application.

## REFERENCES


[1] M. Zhuo, "Cortical plasticity as a new endpoint measurement for chronic pain," *Mol. Pain*, vol. 7, no. 1, pp. 1–14, 2011.

[2] J. K. Krauss et al., "Technology of deep brain stimulation: Current status and future directions," *Nature Rev. Neurol.*, vol. 17, no. 2, pp. 75–87, 2021.

[3] D. K. Biswas, J. H. A. Martinez, J. Daniels, A. Bendapudi, and I. Mahbub, "A novel 3-D printed headstage and homecage based WPT system for long-term behavior study of freely moving animals," in *Proc. IEEE Radio Wireless Symp.*, 2020, pp. 268–271.

[4] D. K. Biswas, J. H. A. Martinez, I. Kaul, A. Kaul, and I. Mahbub, "A miniaturized highly efficient headstage based wireless power transfer (WPT) system for optogenetic stimulation of freely moving animals," in *Proc. IEEE 14th Dallas Circuits Syst. Conf.*, 2020, pp. 1–4.

[5] M. U. Khan, A. Jafar, K. S. Karimov, and S. Feroze, "A proposed optimized solution for wireless power transfer using magnetic resonance coupling," in *Proc. Int. Conf. Intell. Syst. Eng.*, 2016, pp. 350–355.

[6] M. Yuan et al., "Magnetic resonance-based wireless power transfer for implantable biomedical microelectronics devices," in *Proc. IEEE Int. Symp. Signal Process. Inf. Technol.*, 2019, pp. 1–4.

[7] S. Idogawa, K. Yamashita, R. Sanda, R. Numano, K. Koida, and T. Kawano, "A lightweight, wireless bluetooth-low-energy neuronal recording system for mice," *Sensors Actuators B, Chem.*, vol. 331, 2021, Art. no. 129423.

[8] L. U. Daura, G. Tian, Q. Yi, and A. Sophian, "Wireless power transferbased eddy current non-destructive testing using a flexible printed coil array," *Philos. Trans. Roy. Soc. A*, vol. 378, no. 2182, 2020, Art. no. 20190579.

[9] C. A. Balanis, *Antenna Theory: Analysis and Design*. New York, NY, USA: Wiley, 2015.

[10] D. K. Biswas, N. T. Tasneem, and I. Mahbub, "Optimization of miniaturized wireless power transfer system to maximize efficiency for implantable biomedical devices," in *Proc. IEEE Texas Symp. Wireless Microw. Circuits Syst.*, 2019, pp. 1–6.

[11] R. Hinrichs et al., "Sources of magnetic fields," *Physics*, vol. 132, 2020, Art. no. 9.

[12] A. Wolski, "Theory of electromagnetic fields," 2011, *arXiv:1111.4354*.

[13] C. Dichtl, P. Sippel, and S. Krohns, "Dielectric properties of 3D printed polylactic acid," *Adv. Mater. Sci. Eng.*, vol. 2017, 2017, Art. no. 6913835.

[14] D. Semiconductors, "20 V, 2 a very low VF mega schottky barrier rectifier in SOD323 (SC-76) package," PMEG2020AEA Datasheet, Feb. 2004.

[15] U.-M. Jow and M. Ghovanloo, "Design and optimization of printed spiral coils for efficient transcutaneous inductive power transmission," *IEEE Trans. Biomed. Circuits Syst.*, vol. 1, no. 3, pp. 193–202, Sep. 2007.

[16] D. K. Biswas, N. T. Tasneem, and I. Mahbub, "Effects of coaxial-lateral and coaxial-angular displacements on link efficiency of a wirelessly powered optogenetic implant: Design, modeling, and experimental validation," *IEEE J. Electromagn., RF Microw. Med. Biol.*, vol. 3, no. 4, pp. 269–275, Dec. 2019.

[17] M. A. Akram, K.-W. Yang, and S. Ha, "Duty-cycled wireless power transmission for millimeter-sized biomedical implants," *Electronics*, vol. 9, no. 12, 2020, Art. no. 2130.

[18] C. Bargmann et al., "Brain 2025: A scientific vision," 2014. [Online]. Available: http://www.braininitiative.nih.gov/2025/BRAIN2025.pdf

[19] T. Xie and H. Zaidi, "Age-dependent small-animal internal radiation dosimetry," *Mol. Imag.*, vol. 12, no. 6, pp. 7290–2013, 2013.

[20] P. A. Mason, M. R. Murphy, and R. C. Petersen, "IEEE EMF health & safety standards," in *Proc. Asian Ocean Reg. EMF Sci. Meet*, 2001, pp. 1–6.

[21] D. K. Biswas, N. T. Tasneem, and I. Mahbub, "Optimization of miniaturized wireless power transfer system to maximize efficiency for implantable biomedical devices," in *Proc. IEEE Texas Symp. Wireless Microw. Circuits Syst.*, 2019, pp. 1–6.

[22] S. A. Mirbozorgi, H. Bahrami, M. Sawan, and B. Gosselin, "A smart cage with uniform wireless power distribution in 3D for enabling long-term experiments with freely moving animals," *IEEE Trans. Biomed. Circuits Syst.*, vol. 10, no. 2, pp. 424–434, Apr. 2016.

[23] S. Verma, D. Rano, S. Malhotra, and M. S. Hashmi, "Measurements and characterization of a newly developed novel miniature WIPT system," *IEEE Trans. Instrum. Meas.*, vol. 70, 2021, Art. no. 2004211.

[24] B. Lee, M. Kiani, and M. Ghovanloo, "A smart wirelessly powered homecage for long-term high-throughput behavioral experiments," *IEEE Sensors J.*, vol. 15, no. 9, pp. 4905–4916, Sep. 2015.

[25] J. J. Casanova, Z. N. Low, J. Lin, and R. Tseng, "Transmitting coil achieving uniform magnetic field distribution for planar wireless power transfer system," in *Proc. IEEE Radio Wireless Symp.*, 2009, pp. 530–533.

[26] D. K. Biswas, J. H. A. Martinez, J. Daniels, A. Bendapudi, and I. Mahbub, "A novel 3-D printed headstage and homecage based WPT system for long-term behavior study of freely moving animals," in *Proc. IEEE Radio Wireless Symp.*, 2020, pp. 268–271.


**Dipon K. Biswas** (Student Member, IEEE) received the Ph.D. degree from the Department of Electrical Engineering, University of North Texas, Denton, TX, USA. He is currently a Signal Integrity Engineer with Intel Corporation. His research interests include microwave system and antenna design, wireless power transfer, and analog and RF circuit design.

**Nabanita Saha** received the B.Sc. degree in electronics and telecommunication engineering from the Chittagong University of Engineering and Technology (CUET), Bangladesh. She is currently working toward the Ph.D. degree with the Department of Electrical and Computer Engineering, University of Texas at Dallas, Dallas, TX, USA. Her research interests include wireless power transfer, antenna design and optimization, and RF and microwave circuits.

**Ifana Mahbub** (Senior Member, IEEE) received the B.Sc. degree in electrical and electronic engineering from the Bangladesh University of Engineering and Technology, Dhaka, Bangladesh, in 2012, and the Ph.D. degree in electrical engineering from the University of Tennessee, Knoxville, TN, USA, in 2017. She is currently an Assistant Professor and the Texas Instrumentas˜ Early Career Chair Awardee with the Department of Electrical and Computer Engineering, University of Texas at Dallas, Dallas, TX, USA, where she is leading the Integrated Biomedical, RF Circuits, and Systems Laboratory (iBioRFCASL). She has authored or coauthored two book chapters, 29 journal publications, and more than 62 peer-reviewed conference publications. Her research interests include energy-efficient integrated circuits and systems design for read-out, wireless communication, and wireless power transfer for various implantable and wearable sensors. Her current research interests include ultrawideband/mm-wave phased-array antenna design for farfield wireless power transfer/V2V communication for UAVs. Dr. Mahbub was the recipient of the NSF aEarly˜ Career Awarda˜ in 2020, and DARPA aYoung˜ Faculty Awarda˜ in 2021. She was the Publicity Chair of the IEEE Dallas Circuits and Systems Society. She is also the Secretary for the URSI commission K, as the Guest Editor of the IEEE OPEN JOURNAL OF ANTENNAS AND PROPAGATION and *MDPI Sensors Journal*, as a Young Professional Co-Chair of the IEEE Sensors Conference, and as the publications Chair of the IEEE Texas Symposium on Wireless and Microwave Circuits and System and IEEE Dallas Circuits and System Conferences.